

**Provided for non-commercial research and education use.
Not for reproduction, distribution or commercial use.**



This article appeared in a journal published by Elsevier. The attached copy is furnished to the author for internal non-commercial research and education use, including for instruction at the author's institution and sharing with colleagues.

Other uses, including reproduction and distribution, or selling or licensing copies, or posting to personal, institutional or third party websites are prohibited.

In most cases authors are permitted to post their version of the article (e.g. in Word or Tex form) to their personal website or institutional repository. Authors requiring further information regarding Elsevier's archiving and manuscript policies are encouraged to visit:

<http://www.elsevier.com/authorsrights>



Contents lists available at ScienceDirect

Materials Today Physics

journal homepage: <https://www.journals.elsevier.com/materials-today-physics>

Large enhancement of thermoelectric performance in CuInTe₂ upon compression

Hao Yu ^{a, b, c}, Liu-Cheng Chen ^c, Hong-Jie Pang ^c, Xiao-Ying Qin ^a, Peng-Fei Qiu ^d, Xue Shi ^d, Li-Dong Chen ^d, Xiao-Jia Chen ^{c, *}

^a Key Laboratory of Materials Physics, Institute of Solid State Physics, Chinese Academy of Science, Hefei 230031, China

^b University of Science and Technology of China, Hefei 230026, China

^c Center for High Pressure Science and Technology Advanced Research, Shanghai 201203, China

^d State Key Laboratory of High Performance Ceramics and Superfine Microstructure, Shanghai Institute of Ceramics, Chinese Academy of Science, Shanghai 200050, China



HPSTAR
552-2018

ARTICLE INFO

Article history:

Received 8 April 2018

Received in revised form

11 April 2018

Accepted 11 April 2018

Keywords:

Thermoelectricity

Thermal conductivity

High pressure

Electrical and thermal transport

ABSTRACT

Thermoelectric materials can directly generate electric power by converting waste heat, and the efficiency is appraised by the figure of merit zT . A high zT value larger than three is required to achieve comparable efficiency of the traditional heat engines. Despite great efforts for over a century, the desired value of three is seemingly an upper limit, and many existing thermoelectric materials have the zT values less than one. If their zT values can be improved for several times to break through the upper limit, the energy revolution could be expected. Here, a p -type CuInTe₂ is chosen as an example to show the extremely important role of pressure in enhancing the thermoelectric performance. Over five times increase of the zT value is realized by the application of pressure. Both the enhancement of the power factor and the reduction of the thermal conductivity account for this large enhancement. The former is due to the optimization of the carrier concentration and band structure, and the latter is attributed to the enhanced phonon anharmonicity. Our results offer an effective method to improve zT of the existing materials for the future technological applications.

© 2018 Elsevier Ltd. All rights reserved.

With the increasing fossil energy crisis and environment problems, developing alternative energy becomes a major issue. Thermoelectric materials can generate electricity directly from waste heat and are thus considered as renewable energy. Compared with traditional energy, thermoelectric devices are solid-state, noiseless, and environment-friendly. The efficiency of a thermoelectric material is described as a dimensionless figure of merit, $zT = S^2 \rho^{-1} \kappa^{-1} T$, where S is the Seebeck coefficient, T is the absolute temperature, ρ is the electrical resistivity, and κ is the thermal conductivity. A high zT value larger than three is required to make thermoelectric devices commercially viable [1]. The interdependencies of S , ρ , and κ complicate the efforts to improve zT [2,3]. The increasing thirst for new energy attracts the worldwide attentions to develop efficient approaches. To date, numerous materials achieve considerable $zT \sim 1$. The prosperity in turn encourages experimental and theoretical efforts to investigate the

principle of zT enhancement [4–6] and to search for new efficient thermoelectric materials.

The general orientation of recent strategies attempts to optimize the electrical transport properties [7–9] or to reduce the thermal conductivity [10]. In respect to the competition between S and ρ , zT achieves the optimal value [2] within the carrier concentration of $10^{19} \sim 10^{21} \text{ cm}^{-3}$. Doping and alloying, aiming to optimize carrier concentration, usually enhance the electrical transport properties. Heavily doped lead telluride- and bismuth telluride-based materials possess the high zT value ~ 1 for a long time [11–13]. These values were hardly improved until introducing nanostructure to thermoelectric materials. Nanostructuring can significantly reduce thermal conductivity due to the enhancement of boundary scattering and led to the discoveries of rather high $zT \sim 2.2$ in PbTe/SrTe and AgPb_mSbTe_{2+m} [14,15]. In addition to these strategies, some novel approaches and materials were developed on the basis of unique band structure or lattice structure, such as electronic density distortion [16], band convergence effect [17], and materials with complex structure [2]. Meanwhile, pressure has also been

* Corresponding author.

E-mail address: xjchen@hpstar.ac.cn (X.-J. Chen).

recognized to be a powerful means to tune and improve the thermoelectric properties. For examples, a huge improvement of the power of factor has been found by the application of pressure in many materials such as *p*-type $\text{Sb}_{1.5}\text{Bi}_{0.5}\text{Te}_3$ [18] and BaBiTe_3 [19], PbTe -based crystals [20], and Bi_2Te_3 [21]. However, the thermal conductivity was reported to increase with pressure in PbTe [22], seemingly discouraging the high-pressure studies on thermoelectric materials. Recently, a record high $zT \sim 2.6$ was achieved in SnSe single crystals [23]. There is still a long way to go to reach the upper limit. Exploring new strategies to improve zT is highly desired. Here, we choose a *p*-type CuInTe_2 as an example to demonstrate how applying pressure can tune and improve the thermoelectric efficiency based on the development of a series of high-pressure techniques.

CuInTe_2 belongs to the I-III-VI₂ ternary chalcopyrite compounds (I = Cu, Ag; III = Al, Ga, In; and VI = S, Se, Te), sharing a zinc-blende like lattice structure [24] and a multiband structure [25]. It is a promising thermoelectric material [26–28]. The high-pressure thermoelectric parameters of this material were collected based on the technique development by using diamond anvil cells. The cutlet sizes of the diamonds are 300 and 900 μm , respectively. The sample synthesis was detailed previously [26]. All the measurements were repeated twice to check the reproducibility of the data. The obtained results are also compared with the values measured at ambient conditions by using the Physical Properties Measurements System (PPMS) from Quantum Design.

We start to measure the temperature dependence of the electrical and thermal transport properties of CuInTe_2 at ambient pressure by using PPMS. The results are shown in Fig. 1. As can be seen, ρ decreases with increasing temperature over the entire range, exhibiting a typical semiconductor behavior. S behaves in a different way. It sharply increases at the beginning and then quickly reaches saturation value at around 550 $\mu\text{V K}^{-1}$ temperatures above 100 K. Such high S values contribute to good thermoelectric performance at high temperatures by this material. The sign of S is always positive in the whole temperature range measured. This indicates that CuInTe_2 is a *p*-type semiconductor. Around the temperature of 400 K, ρ and S are about $1.1 \times 10^{-2} \Omega\text{m}$ and 557 $\mu\text{V K}^{-1}$, respectively. These values demonstrate that CuInTe_2

possesses high density of states and effective mass. As shown in Fig. 1(c), κ follows a λ shape, the typical behavior for many thermoelectric materials. This has been suggested to result from the grain boundary scattering at low temperatures and three-phonon umklapp process at high temperatures [29]. Here the maximum value of κ is believed to be the result of the crystallite dimension [30]. With increasing temperature, κ is dramatically reduced. These measured quantities yield the monotonous increase of zT to about 2.8×10^{-3} at 400 K.

At temperatures above 100 K, the zT behavior is mainly controlled by κ due to the weak temperature dependence of ρ and the almost saturation of S . It is apparent that the understanding of the κ behavior is crucial for the thermoelectric effect in this material. The total thermal conductivity includes the lattice contribution κ_l and the electron contribution κ_e . Generally, the quantity of κ_e is negligibly small compared to κ_l in a highly efficient thermoelectric material. The lattice conductivity κ_l can be expressed as [31] $\sim (a^4 \delta \theta_D) / (\gamma_G^2 T)$ through the lattice parameter a , material density δ , Debye temperature θ_D , and the phonon Grüneisen parameter γ_G . The contributions of $a^4 \delta$ to κ_l can be simplified to the product of the mass and the lattice parameter because of the expression of the density (mass/volume). With increasing temperature, the lattice usually expands, and the mass remains the constant. Their product cannot decrease κ_l as observed. Meanwhile, Debye temperature θ_D tends to saturate at high temperatures. It cannot account for the decrease of κ_l either. Note that the obtained κ_l slowly declines with increasing temperature rather than decreasing inversely with T . All these factors together indicate that the left phonon Grüneisen parameter should mainly capture the changing trend of κ_l .

Low-frequency phonons usually dominate the behavior of γ_G [23,32]. Low frequencies of phonons mean weak atomic interaction in crystalline materials. Heat always transports through phonons. But weak atomic interaction of phonons could reduce the heat carried by phonons. Thus, the phonons can not transport among the atoms to a long distance due to their weak interaction. If these characteristic phonon frequencies decrease with increasing temperature, the lattice conductivity is expected to reduce. This behavior is often called phonon softening. It is due to the enhanced anharmonic nature of the lattice vibration. This turned out to be the

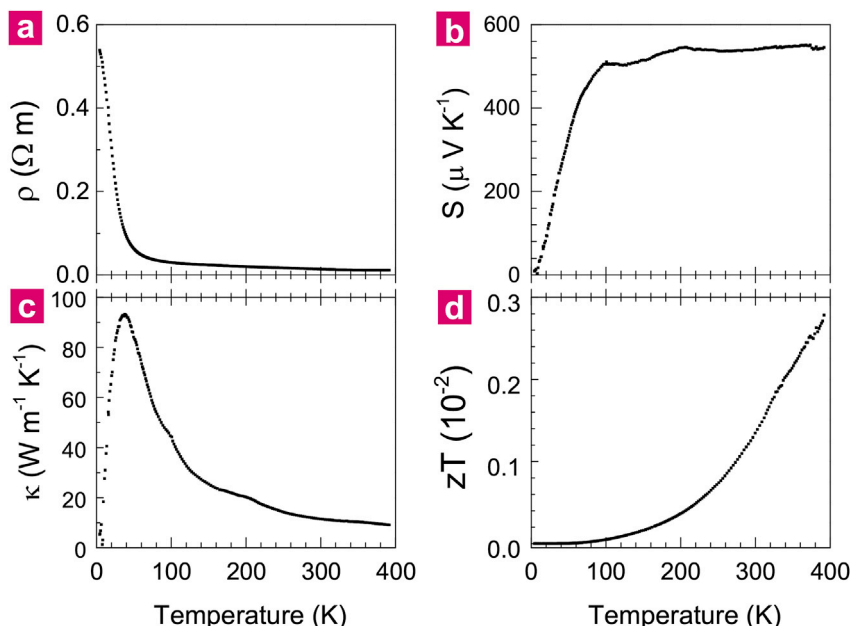


Fig. 1. Temperature dependence of the Seebeck coefficient S (a), the resistivity ρ (b), the thermal conductivity κ (c), and the zT (d) of CuInTe_2 at ambient pressure.

mechanism of the reduction of the thermal conductivity in SnSe [23,32].

Raman scattering spectroscopy is a powerful and effective tool to investigate the zone-center phonons. We have performed low-temperature Raman measurements on CuInTe₂ to investigate the behavior of its zone-center phonons. The sample temperature was controlled from 7 to 300 K in a specially designed cryostat chamber. A 532 nm laser beam was focused on the sample using a 20 times objective to obtain strong signal, and the power was stabilized at 1.5 mW before the objective was used to avoid the localized heating effect. Raman spectra were obtained in a backscattering

configuration, and the results at various temperatures are shown in Fig. 2(a). CuInTe₂ belongs to the space group of D_{2d}^{13} [33]. The lattice modes at Γ point are represented as: $A_1 + 2A_2 + 3B_1 + 3B_2 + 6E$, and all these modes, except A_2 , are Raman active [34]. The spectra exhibit five characteristic phonon bands with the central frequencies, agreeing with those in previous studies [34]. The symmetry assignment of these modes can be determined as B_2^1 , B_1 , E^1 , B_2^2 , and E^2 respectively. The rest modes are hardly observed because of their small Raman cross sections. As seen in Fig. 2(c), the obtained low-frequency phonon modes B_2^1 and B_1 clearly show a softening behavior at temperatures above 100 K. Usually only the

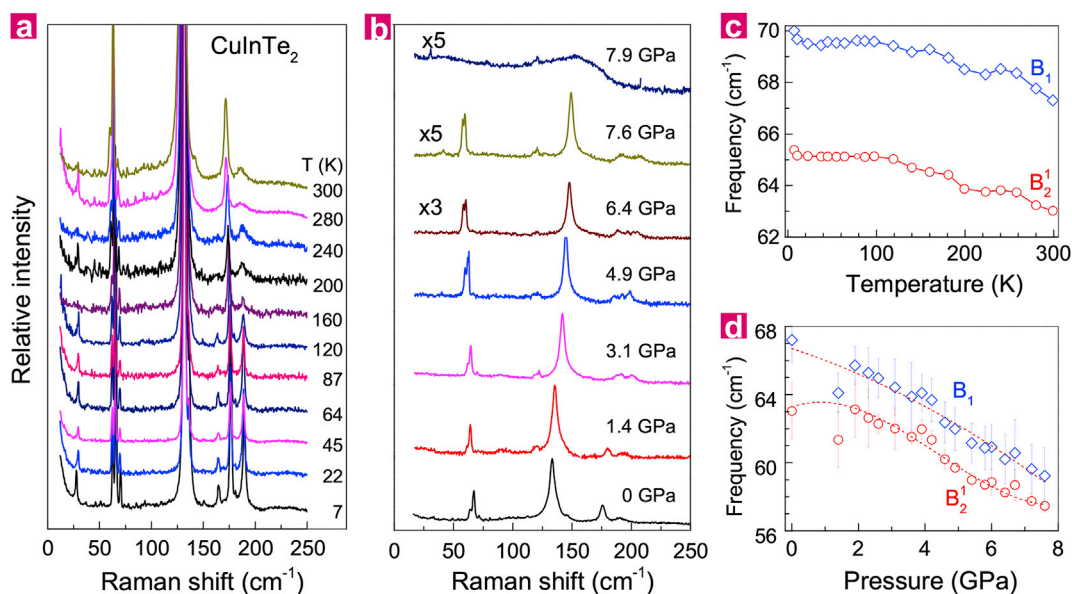


Fig. 2. Raman spectra of CuInTe₂ collected at various temperatures from 7 to 300 K at ambient pressure (a) and at various pressures up to 7.9 GPa at room temperature (b). (c) Temperature dependence of the phonon frequencies of the B₁² and B₁ modes at ambient pressure. (d) Pressure dependence of the phonon frequencies of the B₁² and B₁ modes at room temperature. The data were obtained by the Lorentz fitting to the phonon peaks. The dashed lines in (d) are the guidance to the eye.

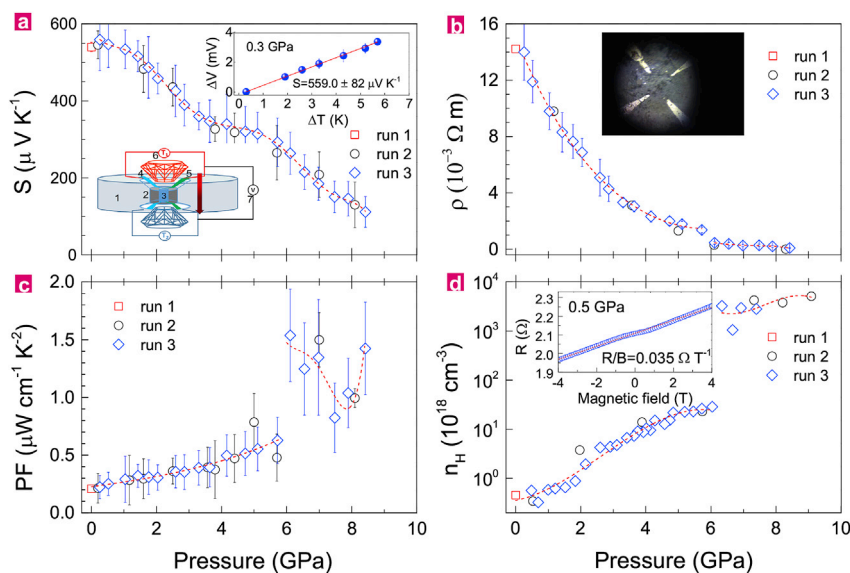


Fig. 3. Pressure dependence of the Seebeck coefficient S (a), the resistivity ρ (b), power factor (c), and charge carrier concentration n_H (d) for CuInTe₂ at room temperature. Run 1 represents the results obtained by PPMS. Run 2 and Run 3 represent the results with different diamond outlet sizes of 300 and 900 μm , respectively. Bottom insert of (a): Diagram of Seebeck coefficient measurement under pressure. 1 denotes gasket, 2 denotes epoxy-BN composite, 3 denotes sample, 4 and 5 are two thermocouples, 6 is temperature sensor, 7 is voltmeter. Top insert of (a): ΔV vs. ΔT at pressure of 0.3 GPa. The linear fitting to the data was used to determine S . Insert of (b): Four electrical leads were attached to the sample. Insert of (d): Hall resistance vs. magnetic field at pressure of 0.5 GPa. The dashed lines are the guidance to the eye. PPMS, Physical Properties Measurements System; PF, power factor.

optical branches of the phonons can be observed from the Raman spectra. In the case of nano-crystalline materials or for the low-frequency modes with overlapping acoustic and optical branches, the obtained low-frequency Raman phonons are valuable to provide the desired phonon information on γ_G . The obtained results support the enhancement of phonon anharmonicity with increasing temperature in this material. Therefore, the increase of zT with temperature above 100 K in the studied material should be mainly controlled by the enhanced phonon anharmonicity. Finding a way to further soften these phonon modes could ensure the further enhancement of zT in this material.

Next we investigate the pressure effects on these thermoelectric parameters. The principle and designed diagram for Seebeck coefficient S measurements are shown in the bottom insert of Fig. 3(a). In such a design, the sample was made in the cylinder shape and was surrounded by the adiabatic pressure medium to ensure the temperature gradient along the axis of the cylinder from the heater (one side) to the cooler (the other side). Measurements of the thermoelectric voltage difference (ΔV) with the applied temperature gradient (ΔT) within 10 K at various pressures were used to calculate S . The top inset of Fig. 3(a) shows the obtained

data at pressure of 0.3 GPa. The obtained results as a function of pressure are summarized in Fig. 3(a). The initial values of S in the 2nd and 3rd runs are about 551 ± 80 and $559.0 \pm 80 \mu V K^{-1}$, respectively, consistent with that in the 1st run. With increasing pressure, S roughly monotonously decreases from the initial value to about $80 \mu V K^{-1}$, exhibiting a strong pressure dependent behavior. The S reduction implies the pressure-induced increase of the carrier concentration and/or the decrease of the density-of-states effective mass.

At high pressures, the ρ was measured by using four-probe method. The electrodes were placed at the top side of the sample as shown in the insert in Fig. 3(b). The obtained ρ values of $CuInTe_2$ as a function of pressure are plotted in Fig. 3(b). As can be seen, ρ is significantly suppressed by the applied pressure. It is decreased to $1.1 \times 10^{-4} \Omega m$ at around 8 GPa. This value is almost two orders in magnitude smaller than that at ambient pressure. The impressively reduced ρ is comparable with that of the optimal doping sample [28]. Such a behavior is similar to S , both indicate a significant modulation of the band structure. Around 6 GPa, the drop of ρ together with the obvious decrease of S implies a possible phase transition. This phase transition has been detected from a high-

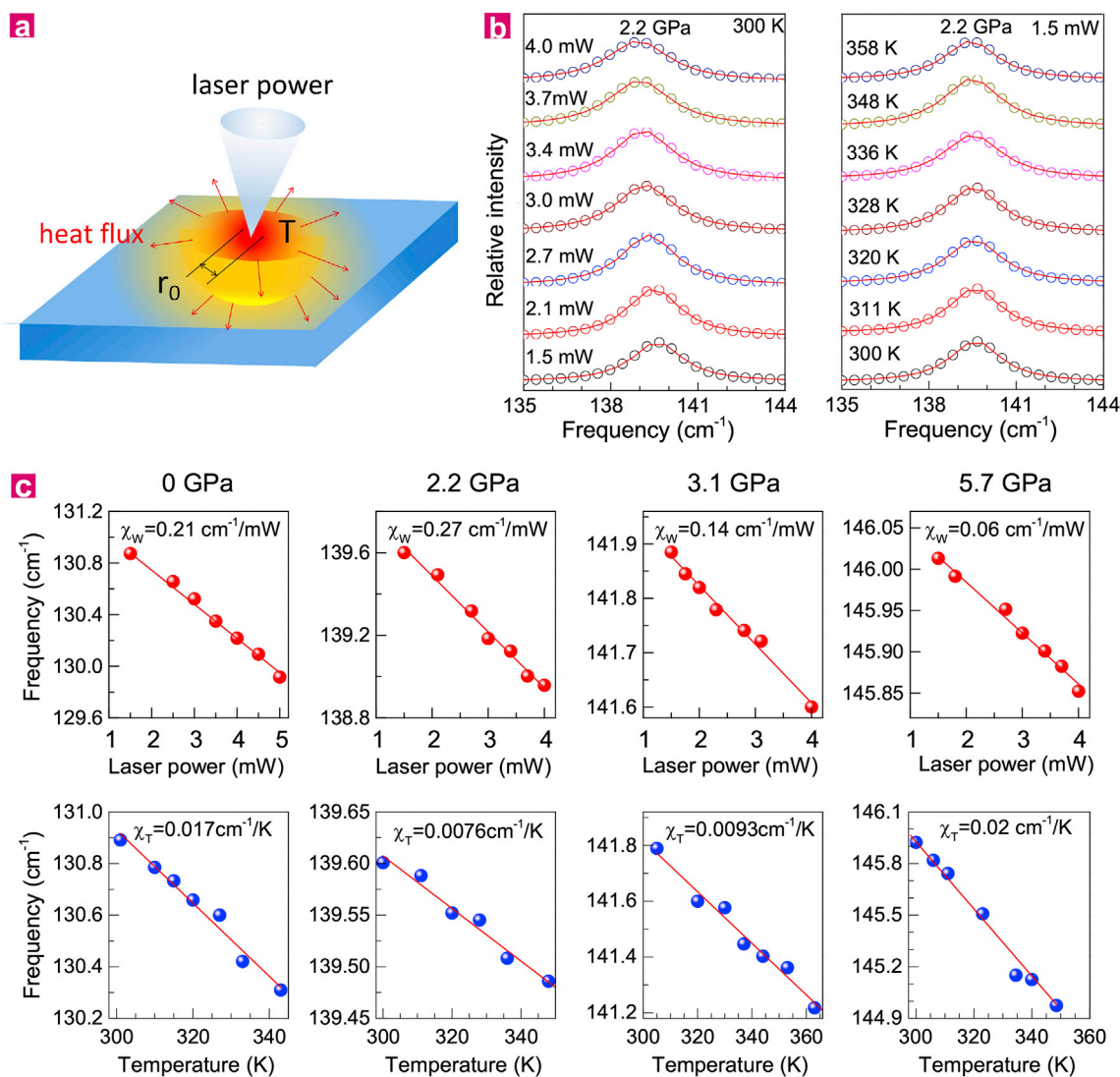


Fig. 4. (a) Diagram for thermal conductivity measurement. (b) Raman spectra of the E_1 mode at pressure of 2.2 GPa measured as functions of temperature and laser power. The phonon frequencies were obtained by Lorentz fitting to the data. (c) Frequencies of the E_1 mode as functions of temperature and laser power at various pressures. χ_T and χ_w were obtained from the linear fitting to the data.

pressure synchrotron X-ray study [35]. The material was found to transform from its initial chalcopyrite phase to the d-Cmcm phase with a volume reduction of 8% at around 6 GPa [35].

Now we are able to calculate the pressure-dependent power factor (PF) by using the formula $PF = S^2/\rho$. The results are plotted in Fig. 3(c). Below 6 GPa, the PF value gradually increases to about 3 times over the ambient pressure value. Above that, PF sharply breaks to an impressive value about $1.5 \mu\text{W cm}^{-1} \text{K}^{-2}$ due to the rapid decrease of ρ . This significant improvement of PF is achieved in a thermoelectric material only through the application of pressure. This finding adds one more example to demonstrate the powerful role of pressure in improving PF for thermoelectric materials [18–22].

The PF behavior mainly reflects the electrical transport properties. Hall effect measurements were taken to give the insight into the pressure effects on these properties. Hall coefficient R_H was obtained by measuring Hall resistance through scanning magnetic fields from -4 Tesla to 4 Tesla at room temperature and each interested pressure. The insert of Fig. 3(d) shows the magnetic field dependence of the Hall resistance at 0.5 GPa. The carrier concentration n_H was thus calculated by using the formula $n_H = 1/eR_H$ based on the pressure dependence of R_H . The results are shown in Fig. 3(d). Here n_H monotonously increases to the ideal value about $3 \times 10^{19} \text{ cm}^{-3}$ around 6 GPa. The improvement of PF and the reduction of S and ρ can be explained by the pressure-induced optimization of n_H . This indicates that applying pressure is able to comprehensively optimize the band structure [36] and n_H . Around 6 GPa, n_H breaks from 2.8×10^{19} to $3.2 \times 10^{21} \text{ cm}^{-3}$. The behaviors of n_H , S , and ρ indicate a phase transition in this compound at 6 GPa, in consistence with the structural study [35].

In order to determine pressure dependence of κ , we developed a technique based on the high-pressure Raman scattering measurements by changing temperatures and laser powers. Similar method has been used to determine the κ of thin films, such as MoS_2 and graphene [37,38]. The focused laser beam will introduce localized heating effect on the cuboid sample, which has been observed previously [39]. Within the ideal thermal transport model shown in Fig. 4(a), κ can be expressed as [37]:

$$\kappa \frac{1}{r} \frac{d}{dr} \left[\frac{1}{r} \frac{T_r}{r} \right] + q(r) = 0$$

where T_r is the temperature distribution, r is the position measured from the heating point, and $q(r)$ is the heat flux distribution. The boundary thermal transport and heat dissipation are neglected in such a model, and the isothermal surface is hemispheric. For the measurements of phonon frequencies with the changes of temperature or laser power, a modified κ expression is simplified by:

$$\kappa = \frac{2\alpha}{\pi r_0} \frac{\chi_T}{\chi_W}$$

where W is the laser power, α is the absorption coefficient of the laser power, r_0 is the width of laser beam on the sample, $\chi_T = \Delta\omega/\Delta T$ ($\chi_W = \Delta\omega/\Delta W$) is the first-order temperature (laser power) derivative of ω , and $\Delta\omega$ is the phonon frequency shift due to the variation of temperature or laser power. Here α is assumed to be insensitive to pressure and can be then estimated from the comparison of the value of κ at ambient pressure measured by other methods. This assumption will not affect the studied trend with pressure. In our measurements, neon was chosen as the pressure transmitting medium. The heat dissipation through neon medium can be safely neglected due to its low κ [40]. Meanwhile, the sample size was chosen to be large enough to avoid the boundary heat

transport. Therefore, the developed technique is capable to give accurate κ value at each pressure and its evolution with pressure.

The E^1 mode of CuInTe_2 exhibits relative strong temperature and laser power–dependent behavior. This mode was thus chosen to calculate κ . Fig. 4(b) shows the Raman spectra of the E^1 mode at 2.2 GPa collected at different temperatures with a fixed laser power or by changing laser powers at a fixed temperature. The obtained frequencies from Lorentz fitting to the data are plotted in Fig. 4(c) as functions of temperature and laser power at various pressures. χ_T and χ_W were thus determined by the linear fitting to the data for each pressure. Based on the measured r_0 and the obtained α from the comparison of the ambient pressure κ value measured by PPMS, we obtained the pressure dependence of κ for CuInTe_2 [Fig. 5(a)]. With increasing pressure, κ is significantly reduced from $11.7 \text{ Wm}^{-1} \text{K}^{-1}$ to a minimum value of $4.1 \text{ Wm}^{-1} \text{K}^{-1}$. It remains at relative low values at high pressures. Above 6 GPa, a modest increase of κ is observed when the material enters a new phase [35]. The pressure level for the κ anomaly is almost the same as ρ and n_H , again indicating the phase transition. The pressure-induced reduction of κ at low pressures is a surprising discovery of this work.

Raman spectra were again collected at pressures up to 7.9 GPa to understand the κ reduction, especially the expected phonon softening as indicated before. The collected spectra at room temperature at various pressures are shown in Fig. 2(b). Indeed, the two low-frequency phonon modes B^1 and B^2 roughly exhibit anomalous softening. The softening of these modes can be clearly seen in Fig. 2(d). Pressure-induced phonon anharmonicity therefore becomes the leading mechanism to account for the reduction of κ in this material. Above 6 GPa, the phonon intensities are significantly reduced and almost vanished around 8 GPa. This again coincides with the phase transition reported previously [35].

Now that the pressure dependences of S , ρ , and κ have been determined, we are able to obtain the evolution of zT with pressure

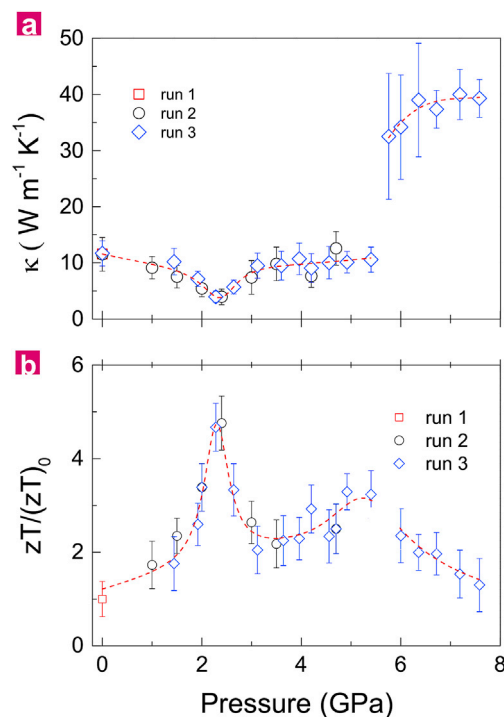


Fig. 5. Pressure dependence of the κ (a) and zT (b) for CuInTe_2 . The value of zT is normalized by the atmospheric pressure value (about 1.2×10^{-3}). The dashed lines are the guidance to the eye.

for CuInTe_2 . The results are summarized in Fig. 5(b). Here the zT values at high pressures are normalized to the value at ambient pressure. With increasing pressure, $zT/(zT)_0$ gradually increases and exhibits a maximum around 2.5 GPa. The maximum of zT value is about five times higher than that at ambient pressure. Pressure is proved to induce the collaboration of enhanced PF and significantly reduce κ . These results reveal that the impressive improvements come from the optimization of band structure and the enhancement of phonon anharmonicity. These advantages provide extra contributions going beyond the adverse effect from traditional methods. Significant zT improvements of existing thermoelectric materials can be expected at high pressures. The date to break up the upper zT limit of three should be not that far.

Acknowledgments

Xun Shi and Li-Dong Chen acknowledged the support from the Key Research Program of Chinese Academy of Sciences under Project No. KFZD-SW-421, the Natural Science Foundation of China under the No. 51625205, and the Shanghai Government (Grant No. 16XD1403900). Xiao-Ying Qin acknowledged the support from the Natural Science Foundation of China under Grant Nos. 51672278, 11674322, and 11374306.

References

- [1] Z.F. Ren, Y.C. Lan, Q.Y. Zhang, *Advanced Thermoelectrics: Materials, Contacts, Devices, and Systems*, CRC Press, 2017.
- [2] G.J. Snyder, E.S. Toberer, Complex thermoelectric materials, *Nat. Mater.* 7 (2008) 105–114.
- [3] H. Alam, S. Ramakrishna, A review on the enhancement of figure of merit from bulk to nano-thermoelectric materials, *Nano Energy* 2 (2013) 190–212.
- [4] W.S. Liu, J.Z. Hu, S.M. Zhang, M.J. Deng, C.G. Han, Y. Liu, New trends, strategies and opportunities in thermoelectric materials: a perspective, *Mater. Today Phys.* 1 (2017) 50–60.
- [5] C. Chang, L.D. Zhao, Anharmonicity and low thermal conductivity in thermoelectrics, *Mater. Today Phys.* 4 (2018) 50–57.
- [6] Q.C. Song, T.H. Liu, J.W. Zhou, Z.W. Ding, G. Chen, Ab initio study of electron mean free paths and thermoelectric properties of lead telluride, *Mater. Today Phys.* 2 (2017) 69–77.
- [7] J. Mao, Y.X. Wu, S.W. Song, J. Shuai, Z.H. Liu, Y.Z. Pei, Z.F. Ren, Anomalous electrical conductivity of n-type Te-doped $\text{Mg}_{3.2}\text{Sb}_{1.5}\text{Bi}_{0.5}$, *Mater. Today Phys.* 3 (2017) 1–6.
- [8] Z.H. Liu, J. Mao, S.Y. Peng, B.Q. Zhou, W.H. Gao, J.H. Sui, Y.Z. Pei, Z.F. Ren, Tellurium doped n-type $\text{Zr}_{3.2}\text{Ni}_{3.2}\text{Sb}_4$ thermoelectric materials: Balance between Carrier-scattering mechanism and bipolar effect, *Mater. Today Phys.* 2 (2017) 54–61.
- [9] R. He, H.T. Zhu, J.Y. Sun, J. Mao, H. Reith, S. Chen, G. Schierning, K. Nielsch, Z.F. Ren, Improved thermoelectric performance of n-type half-Heusler $\text{MCo}_{1-x}\text{Ni}_x\text{Sb}$ ($M = \text{Hf, Zr}$), *Mater. Today Phys.* 1 (2017) 24–30.
- [10] K.P. Zhao, P.F. Qiu, Q.F. Song, A.B. Blichfeld, E. Eikeland, D.D. Ren, B.H. Ge, B.B. Iversen, X. Shi, L.D. Chen, Ultrahigh thermoelectric performance in $\text{Cu}_{2-x}\text{Se}_{0.5}\text{S}_{0.5}$ liquid-like materials, *Mater. Today Phys.* 1 (2017) 14–23.
- [11] Y.Z. Pei, A. Lalonde, S. Iwanaga, G.J. Snyder, High thermoelectric figure of merit in heavy hole dominated PbTe , *Energy Environ. Sci.* 4 (2011) 2085–2089.
- [12] H.J. Goldsmid, Bismuth telluride and its alloys as materials for thermoelectric generation, *Materials* 7 (2014) 2577–2592.
- [13] Y.H. Wu, R.S. Zhai, T.J. Zhu, X.B. Zhao, Enhancing room temperature thermoelectric performance of n-type polycrystalline bismuth-telluride-based alloys via Ag doping and hot deformation, *Mater. Today Phys.* 2 (2017) 62–68.
- [14] K. Biswas, J. He, I.D. Blum, C.I. Wu, T.P. Hogan, D.N. Seidman, V.P. Dravid, M.G. Kanatzidis, High-performance bulk thermoelectrics with all-scale hierarchical architectures, *Nature* 489 (2012) 414–418.
- [15] K.F. Hsu, S. Loo, F. Guo, W. Chen, J.S. Dyck, C. Uher, T. Hogan, E.K. Polychroniadis, M.C. Kanatzidis, Cubic $\text{AgPb}_m\text{SbTe}_{2+m}$: bulk thermoelectric materials with high figure of merit, *Science* 35 (2004) 818–821.
- [16] J.P. Heremans, V. Jovovic, E.S. Toberer, A. Saramat, K. Kurosaki, A. Charoenphakdee, S. Yamanaka, G.J. Snyder, Enhancement of thermoelectric efficiency in PbTe by distortion of the electronic density of states, *Science* 321 (2008) 554–557.
- [17] Y.Z. Pei, X. Shi, A. Lalonde, H. Wang, L.D. Chen, G.J. Snyder, Convergence of electronic bands for high performance bulk thermoelectrics, *Nature* 473 (2011) 66–69.
- [18] D.A. Polvani, J.F. Meng, N.V. Chandra Shekar, J. Sharp, J.V. Badding, Large improvement in thermoelectric properties in pressure-tuned p-type $\text{Sb}_{1.5}\text{Bi}_{0.5}\text{Te}_3$, *Chem. Mater.* 13 (2001) 2068–2071.
- [19] J.F. Meng, N.V. Chandra Shekar, J.V. Badding, D.Y. Chung, M.G. Kanatzidis, Multifold enhancement of the thermoelectric figure of merit in p-type BaBiTe_3 by pressure tuning, *J. Appl. Phys.* 90 (2001) 2836–2839.
- [20] S.V. Ovsyannikov, V.V. Shchennikov, Pressure-tuned colossal improvement of thermoelectric efficiency of PbTe , *Appl. Phys. Lett.* 90 (2007) 122103.
- [21] S.V. Ovsyannikov, V.V. Shchennikov, G.V. Vorontsov, A.Y. Manakov, A.Y. Likhacheva, V.A. Kulbachinskii, Giant improvement of thermoelectric power factor of Bi_2Te_3 under pressure, *J. Appl. Phys.* 104 (2008) 053713.
- [22] M.K. Jacobsen, R.S. Kumar, A.L. Cornelius, Transport properties of Ni and PbTe under pressure, *J. Electron. Mater.* 41 (2012) 633–638.
- [23] L.D. Zhao, S.H. Lo, Y. Zhang, H. Sun, G. Tan, C. Uher, C. Wolverton, V.P. Dravid, M.G. Kanatzidis, Ultralow thermal conductivity and high thermoelectric figure of merit in SnSe crystals, *Nature* 508 (2014) 373–377.
- [24] J.L. Shay, J.H. Wernick, *Ternary Chalcopyrite Semiconductors: Growth, Electronic Properties and Applications*, Pergamon Press, New York, 1975.
- [25] G. Zhou, D. Wang, High thermoelectric performance from optimization of hole-doped CuInTe_2 , *Phys. Chem. Chem. Phys.* 18 (2016) 5925–5931.
- [26] R. Liu, L. Xi, H. Liu, X. Shi, W. Zhang, L.D. Chen, Ternary compound CuInTe_2 : a promising thermoelectric material with diamond-like structure, *Chem. Commun.* 48 (2012) 3818–3820.
- [27] A. Kosuga, T. Plirdpring, R. Higashine, M. Matsuzawa, K. Kurosaki, S. Yamanaka, High-temperature thermoelectric properties of $\text{Cu}_{1-x}\text{In}_x\text{Te}_2$ with a chalcopyrite structure, *Appl. Phys. Lett.* 100 (2012) 042108.
- [28] N. Cheng, R. Liu, S. Bai, X. Shi, L.D. Chen, Enhanced thermoelectric performance in Cd doped CuInTe_2 compounds, *J. Appl. Phys.* 115 (2014) 163705.
- [29] M.G. Holland, Analysis of lattice thermal conductivity, *Phys. Rev.* 132 (1963) 2461–2471.
- [30] J. Callaway, Model for lattice thermal conductivity at low temperatures, *Phys. Rev.* 113 (1959) 1046–1051.
- [31] C. Gayner, K.K. Kar, Recent advances in thermoelectric materials, *Prog. Mater. Sci.* 83 (2016) 330–382.
- [32] C.W. Li, J. Hong, A.F. May, D. Bansal, S. Chi, T. Hong, G. Ehlers, O. Delaire, Orbitally driven giant phonon anharmonicity in SnSe , *Nat. Phys.* 11 (2015) 1063–1069.
- [33] A.M. Mintairov, N.A. Sadchikov, T. Sauncy, M. Holtz, G.A. Seryogin, S.A. Nikishin, H. Temkin, Vibrational Raman and infrared studies of ordering in epitaxial ZnSnP_2 , *Phys. Rev. B* 59 (1999) 15197.
- [34] C. Rincón, S.M. Wasim, G. Marín, E. Hernández, J. Galibert, Raman spectra of the chalcopyrite compound CuGaTe_2 , *J. Appl. Phys.* 62 (2001) 847–855.
- [35] Y. Mori, T. Ikai, K. Takarabe, High-pressure phase in the chalcopyrites CuGaTe_2 and CuInTe_2 , *Phys. Stat. Solidi(b)* 235 (2003) 317–320.
- [36] G.J. Tan, L.D. Zhao, F.Y. Shi, J.W. Doak, S.H. Lo, H. Sun, C. Wolverton, V.P. Dravid, C. Uher, M.G. Kanatzidis, High thermoelectric performance of p-type SnTe via a synergistic band engineering and nanostructuring approach, *J. Am. Chem. Soc.* 136 (2014) 7006–7017.
- [37] R. Yan, J.R. Simpson, S. Bertolazzi, J. Brivio, M. Watson, X. Wu, A. Kis, T. Luo, A.R. Hight Walker, H.G. Xing, Thermal conductivity of monolayer molybdenum disulfide obtained from temperature-dependent Raman spectroscopy, *ACS Nano* 8 (2014) 986–993.
- [38] W. Cai, A.L. Moore, Y. Zhu, X. Li, S. Chen, L. Shi, R.S. Ruoff, Thermal transport in suspended and supported monolayer graphene grown by chemical vapor deposition, *Nano Lett.* 10 (2010) 1645–1651.
- [39] S. Najmaei, Z. Liu, P.M. Ajayan, J. Lou, Thermal effects on the characteristic Raman spectrum of molybdenum disulfide (MoS_2) of varying thicknesses, *Appl. Phys. Lett.* 100 (2012) 013106.
- [40] J.V. Sengers, W.T. Bolk, C.J. Stigter, The thermal conductivity of neon between 25°C and 75°C at pressures up to 2600 atmospheres, *Physica* 30 (1964) 1018–1026.